Three-dimensional transient channel flow at moderate Reynolds numbers: Analysis and wall modeling

By M. G. Giometto, A. Lozano-Durán, G. I. Park AND P. Moin

1. Motivation and objectives

Our current understanding of wall-bounded turbulent flows is rooted largely in studies of equilibrium wall turbulence. Townsend (1961) was the first to coin the term "equilibrium layer" to define a portion of boundary layer in which the rates of production and destruction of turbulent kinetic energy are equal. This definition implied the existence of layers through which the stress has a linear relation with distance from the wall, and it did not necessarily exclude the flows with mean acceleration and streamwise pressure gradients. Later, DeGraaff and Eaton (2000) suggested a more restrictive definition of equilibrium boundary layer where the total shear stress is in equilibrium with the shear stress at the wall. More recently, Maciel *et al.* (2006) presented a consistent theory of self-similarity and of equilibrium in the outer region of turbulent boundary layers that explains recent experimental findings on the subject.

A vast majority of the fundamental studies on wall turbulence indeed have investigated this narrower subset of equilibrium wall-bounded flows, focusing on flows in/over plane channels, pipes, and flat plates. These studies have unraveled several fundamental characteristics of near-wall turbulence, such as the self-sustaining cycle of wall turbulence, dominant coherent structures in increasingly high Reynolds number boundary layers, their geometry and life cycle, the wall-attached hierarchy of turbulent eddies, and its overall implication on energy cascade and log-layer dynamics (Jiménez & Pinelli 1999; Panton 2001; Flores & Jiménez 2010; Hwang & Cossu 2011; Lozano-Durán *et al.* 2012; Lozano-Durán & Jiménez 2014; Cossu & Hwang 2017).

Unfortunately, the knowledge and theories built upon equilibrium wall turbulence have had limited impact on our ability to predict practical flows of interest. This is because spatial homogeneity and unidirectional shear, which are the basic assumptions required to attain equilibrium, are absent in such flows. Instead, turbulence in engineering flows is strongly affected by non-equilibrium effects controlled by flow-dependent boundary conditions. Consequently, the law-of-the-wall, scaling laws, and reduced-order models established largely for equilibrium turbulent boundary layer cannot be generalized to non-canonical flows. Additionally, rapid variations in the strain and vorticity, often present in such flows, render many turbulence closure models calibrated to equilibrium turbulence of limited utility.

One class of such non-equilibrium flows, with particular relevance to external aerodynamics and hydrodynamics, is that of turbulent boundary layers with mean-flow three dimensionality. For instance, three-dimensional turbulent boundary layers (3DTBL) are more the rule than the exception in the swept-back wings in aerial vehicles, the stern/bow regions of ships, and submarine hulls. In these flows, the mean flow direction changes continuously across the shear-layer thickness due to the cross-stream pressure gradient

induced by the geometry of the immersed body. Fundamental questions remain unanswered with regard to changes of wall-turbulence structure with the imposition of extra rates of mean strain, and on the effects these changes have on the turbulence production and destruction mechanisms. These manifest themselves in distinctive behaviors of 3DTBL such as diminution of the turbulent shear stress with imposition of additional cross-stream strain and misalignment of the Reynolds shear stress and the mean shear. These characteristics pose challenges to many turbulence models based on isotropic eddy viscosity.

The majority of the experimental works concerning 3DTBL are summarized in the review of Johnston & Flack (1996). Computational studies carried out to date include 3DTBLs found in the plane channel (Moin *et al.* 1990; Coleman & Spalart 1996), flat plate (Kiesow & Plesniak 2003; Spalart 1989), rotating disk (Littell & Eaton 1994; Wu & Squires 2000), and concentric annulus at low Reynolds number flows, where more than half of the boundary layer is dominated by the viscous wall effect. However, distinctly different mechanisms may be at work in higher Reynolds number flows in which the inviscid core region would occupy a considerable portion of the boundary layer. With this motivation, this report lays the groundwork for an improved understanding of non-equilibrium processes in 3DTBL.

Using direct numerical simulation (DNS), we study temporally developing 3DTBLs in a planar channel at friction Reynolds numbers from 186 up to 934 subjected to a range of spanwise forcing. This flow is well suited for the study of the near-wall three dimensionality due to its simple geometry. Note that the cross-stream strain in the channel flow is generated solely by viscous diffusion from the wall, while it is generated primarily by the inviscid skewing mechanism in external aerodynamics applications. However, characteristic behaviors of 3DTBL are thought be similar irrespective of the source of three dimensionality (Moin *et al.* 1990). This aspect will be investigated in a separate study planned for the upcoming year, where a spatially developing 3DTBL in a bent square duct will be analyzed in detail.

The primary foci of this report are a consideration of the inner and outer scalings in 3DTBLs (which were absent in previous studies at low Reynolds numbers), an analysis of the effects of variable spanwise forcing magnitude on the Reynolds stress deficit, and an elucidation of the role of viscous and inviscid mechanisms on turbulence during the initial transient. Additionally, the predictive capability of state-of-the-art wall-modeling techniques for large-eddy simulation (LES) will be assessed in 3DTBLs for the first time under the proposed controlled scenario. The relatively simple flow setup entails some of the core features of 3DTBL, and is hence expected to challenge available wall-closure formulations within a framework that facilitates the analysis.

To date, a large number of studies has focused on the development and testing of wall-layer models for LES, motivated by the need to bypass the inner wall region and reduce computational costs (Chapman 1979; Choi & Moin 2012). Early models relying on equilibrium assumptions work fairly well in simple flows for which they were calibrated, but are known to fail in a range of complex flows scenarios (Larsson 2016). This has motivated recent efforts to account for non-equilibrium effects, which yield a robust behavior over a number of non-canonical flow setups (see for instance the recent review by Bose & Park 2018). Note that in general wall-layer models are not very effective at transferring information from the inner to the outer layer, i.e. they tend to be more accurate when the inner/outer-layer interaction is one-way, with the outer layer supplying the forcing (Piomelli & Balaras 2002). The current flow, characterized by a spanwise

Re_τ	L_1/h	L_3/h	Δ_1^+	Δ_3^+	$\Delta_{2,max}^+$	$\Delta_{2,min}^+$	N_2	Tu_τ/h	$P_{,x_3}/P_{,x_1}$
186	4π	2π	9.05	4.52	6.4	0.32	259	1	1 to 125
546	4π	2π	8.92	4.46	6.2	0.30	385	1	40
934	8π	3π	7.36	4.29	6.7	0.35	801	1	10

TABLE 1. Geometry and parameters for the reference DNS runs. $Re_\tau = h^+$ is the friction Reynolds number. L_1 and L_3 are the streamwise and spanwise dimensions of the numerical box and h is the channel half-width. $\Delta_1^+ \equiv \Delta_1 u_\tau/\nu$ and Δ_3^+ are the spatial grid resolutions in the streamwise and spanwise directions in inner units. $\Delta_{2,min}^+$ and $\Delta_{2,max}^+$ are the finer and coarser grid stencil in the wall-normal direction (a stretched grid in the wall-normal direction is adopted). N_y is the number of wall-normal collocation points. Simulations are integrated in time for one eddy turnover Tu_τ/h. A single spanwise pressure gradient $\mathrm{d}P/\mathrm{d}x_3$ is used for the $Re_\tau = 934$ and $Re_\tau = 546$ cases, whereas a range of $\mathrm{d}P/\mathrm{d}x_3$ are considered for cases at $Re_\tau = 186$.

boundary layer growing from the wall due to viscous effects, is hence expected to be challenging to reproduce for WMLES.

The brief is organized as follows: in Section 2 an analysis of DNS results is proposed, Section 3 will focus on the comparison of selected quantities between DNS and wall-modeled LES, and conclusions will follow in Section 4.

2. Analysis of DNS data

2.1. *Numerical setup*

A series of DNS of fully-developed incompressible planar channel flows are performed, with focus on the initial transient after a sudden transverse pressure gradient is applied. Three Reynolds numbers are considered, namely $Re_\tau = hu_\tau/\nu = 186$, $Re_\tau = 546$, and $Re_\tau = 934$, where h is the channel half-height, u_τ is the friction velocity and ν is the kinematic viscosity. Wall (or inner) units, $(\cdot)^+$, are defined in terms of u_τ and ν. Outer units, $(\cdot)^*$, are obtained by normalizing with u_τ and h. The streamwise, wall-normal and spanwise directions are represented by x_1, x_2 and x_3, respectively, and the corresponding velocities are u_1, u_2 and u_3. Simulations are initialized from a fully-developed equilibrium planar channel flow at the corresponding Reynolds number, and a set of constant mean spanwise pressure gradients $\mathrm{d}P/\mathrm{d}x_3$ are considered.

A fully staggered second-order accurate centered finite difference method (Orlandi 2000) is employed in space, time advancement is performed via a third-order accurate Runge-Kutta method (Wray 1990), and the system of equations is solved via an operator splitting approach (Chorin 1968). Details on the setup of simulations are provided in Table 1. A single run with $\mathrm{d}P/\mathrm{d}x_3 = 10\mathrm{d}P/\mathrm{d}x_1$ and $\mathrm{d}P/\mathrm{d}x_3 = 40\mathrm{d}P/\mathrm{d}x_1$ is performed for the $Re_\tau = 934$ and $Re_\tau = 546$ channel flow cases, respectively, whereas a range of $\mathrm{d}P/\mathrm{d}x_3$ are considered for cases at $Re_\tau = 186$. To converge statistics during the initial transient, ensemble averaging is performed over 20, 10 and 2 runs for the $Re_\tau = 186$, $Re_\tau = 546$ and $Re_\tau = 934$ cases, respectively. Each calculation is initialized with time-decorrelated velocity snapshots from the corresponding two-dimensional fully-developed equilibrium planar channel flow. Averaging is also performed in the spatial homogeneous

directions and over the top and bottom halves of the channel. The averaging operator is hereafter denoted by $\overline{(\cdot)}$.

2.2. *Results and discussion*

The focus of this section is on the initial transient period after the spanwise pressure gradient is imposed, as the flow eventually degenerates to an equilibrium two-dimensional channel flow. Previous numerical studies and experiments have reported a decrease in the turbulent kinetic energy and in the turbulent shear stress as equilibrium boundary layers undergo rapid spanwise straining (Moin *et al.* 1990; Coleman *et al.* 1996; Johnston & Flack 1996). In particular, the study by Moin *et al.* (1990) – which shares the same setup of the current study – showed that the $\overline{u_1 u_2}$ Reynolds stress component experiences a decrease during an initial transient of duration $T^* = 1$ ($T^+ = 186$), after a sudden spanwise pressure gradient $\mathrm{d}P/\mathrm{d}x_3 = 10\mathrm{d}P/\mathrm{d}x_1$ is imposed. In the current section, the analysis from Moin *et al.* (1990) is extended by providing the Reynolds number scaling of the $\overline{u_1 u_2}$ variations and by investigating its dependence for different $\mathrm{d}P/\mathrm{d}x_3$. The mechanisms responsible for the observed decrease in $|\overline{u_1 u_2}|$ are also discussed.

2.2.1. *Scaling analysis*

In fully-developed, pressure-driven channel flows it is customary to scale the governing equations in wall units when the focus is on the near-wall region (where $x_2 = \mathcal{O}(\nu/u_\tau)$), and in outer units, u_τ and h, when attention is paid to on the outer flow regions (where $x_2 = \mathcal{O}(h)$). These parameters make the leading-order inner and outer form of the governing equations invariant with respect to Re_τ, and a qualitative collapse of the resulting solutions is therefore expected for numerical experiments at different Re_τ. For the problem under consideration, a new dimensional parameter is introduced in the momentum conservation equations, namely the magnitude of the spanwise pressure gradient, which results in an additional dimensionless parameter upon normalization.

Adopting the customary inner units to normalize the governing equations in the near-wall region, i.e. all such regions where $x_2 \sim \nu/u_\tau$, the momentum conservation equations for the system read

$$\frac{Du_i^+}{Dt^+} = -\frac{\partial \pi^+}{\partial x_i^+} - \frac{\delta_{i1}}{Re_\tau} - \frac{w_\tau^{2\,+}}{Re_\tau}\delta_{i2} + \frac{\partial^2 u_i^+}{\partial x_i^{2\,+}}\,, \tag{2.1}$$

where $\pi \equiv p/\rho$ is the kinematic pressure, ρ is a constant reference density, and where $w_\tau = \sqrt{h(\mathrm{d}P/\mathrm{d}x_3)}$ is the spanwise friction velocity. For the initial equilibrium channel flow, Re_τ effects can be regarded as a higher-order correction to the flow field in the near-wall region, and hence runs characterized by different Re_τ but the same $(\mathrm{d}P/\mathrm{d}x_3)^+ \equiv w_\tau^{2\,+}/Re_\tau$ are expected to show a qualitative collapse of statistics at $x_2^+ = \mathcal{O}(1)$ during the initial transient. Note that an exact collapse of statistics ($\overline{u_i}$, $\overline{u_i u_j}$, etc.) is not possible, as the resulting equations are indeterminate owing to the appearance of higher-order terms which are usually dominant balance terms at selected subregions (Klewicki *et al.* 2007).

When considering the flow region $x_2 \sim h$, the natural choice of normalization for the equations of motion are outer units. The normalized momentum conservation equations in this case read

$$\frac{Du_i^*}{Dt^*} = -\frac{\partial \pi^*}{\partial x_i^*} - \delta_{i1} - (w_\tau^*)^2\delta_{i2} + \frac{1}{Re_\tau}\frac{\partial^2 u_i^*}{\partial x_i^{2\,*}}\,. \tag{2.2}$$

As apparent from Eq. (2.2), the leading-order outer form of the equations for the initial equilibrium channel flow does not depend on Re_τ (viscous terms are of order $1/Re_\tau \ll 1$),

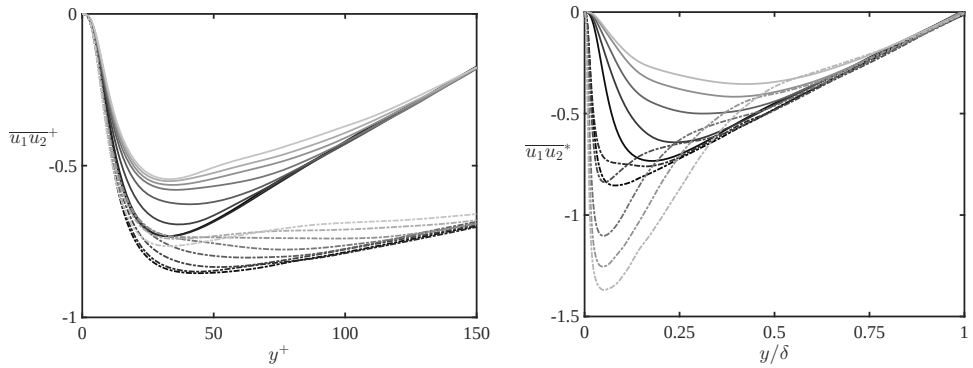

FIGURE 1. Left: Time evolution of the spatial- and ensembled-averaged Reynolds shear stress $\overline{u_1u_2}^+$ for channel flow simulations characterized by $(\mathrm{d}P/\mathrm{d}x_3)^+ \equiv w_\tau^{2+}/Re_\tau = 7.3 \times 10^{-2}$ at $Re_\tau = 186$ (solid lines) and $Re_\tau = 546$ (dot-dashed lines). Note that $(\mathrm{d}P/\mathrm{d}x_3)^+ = 7.3 \times 10^{-2}$ for the $Re_\tau = 546$ corresponds to $\mathrm{d}P/\mathrm{d}x_3 = 40\mathrm{d}P/\mathrm{d}x_1$. The displayed profiles are $\Delta t^+ = 12$ apart and light gray lines correspond to approximately 1/2 eddy-turnover time for the $Re_\tau = 186$ case ($T^+ = 96$). Right: Time evolution of the spatial- and ensembled-averaged Reynolds shear stress $\overline{u_1u_2}^*$ for channel flow simulations characterized by $(\mathrm{d}P/\mathrm{d}x_3)^* \equiv w_\tau^{2*}/1 = 40$ at $Re_\tau = 186$ (solid lines) and $Re_\tau = 546$ dot-dashed lines. The displayed time intervals correspond to $\Delta t^* = 0.2$ and light gray lines denote time $t = 0$.

and hence runs characterized by different Re_τ, but the same w_τ^* are expected to show a qualitative collapse of turbulence statistics during the initial transient at $x_2/h = \mathcal{O}(1)$ under such scaling.

As revealed by Figure 1, the proposed scaling collapses well the initial time-transient of the space- and ensemble-averaged $\overline{u_1u_2}$ in both the inner and outer layers when the appropriate repeating parameters are adopted. Specifically, runs at different Re_τ but the same $(\mathrm{d}P/\mathrm{d}x_3)^+$ feature a similar decrease in $|\overline{u_1u_2}|^+$ in the near-wall regions for corresponding Δt^+ variations, and runs at different Re_τ but the same w_τ/u_τ ratio feature a similar reduction in $|\overline{u_1u_2}|^+$ in the outer layer for equal Δt^* variations.

In the former cases, $|\overline{u_1u_2}|^+$ is found to decrease throughout initial transient $T^+ = 186$, which corresponds to half eddy turnover time for the lowest among the considered Re_τ. When scaled with inner units based on u_τ and ν the near-wall collapse and scaling between solutions at different Re_τ is only qualitative, as qualitative as the collapse of near-wall statistics in two-dimensional equilibrium channel flows at different Re_τ.

In contrast, runs characterized by different Re_τ but the same $(\mathrm{d}P/\mathrm{d}x_3)^*$ feature an excellent collapse of the corresponding $|\overline{u_1u_2}|^*$ time evolution at $x_2/h = \mathcal{O}(1)$ when scaled in outer units, whereas under the same scaling, contrasting trends are observed in the near-wall regions ($x_2 \lesssim 0.4h$). Interestingly, for a transient duration of $T^* = 1$, the magnitude of $|\overline{u_1u_2}|^*$ is found to increase in the near-wall regions for the $Re_\tau = 546$ cases, whereas it decreases for the $Re_\tau = 186$ runs. Such a behavior can be better understood when considering that near-wall dynamics scale in inner units, as discussed in the previous section, hence the recovery of the near-wall boundary-layer towards the new equilibrium condition – characterized by larger $|\overline{u_1u_2}|^*$ – occurs more rapidly for higher Reynolds number flows when measured in outer time units for a given $(\mathrm{d}P/\mathrm{d}x_3)^*$.

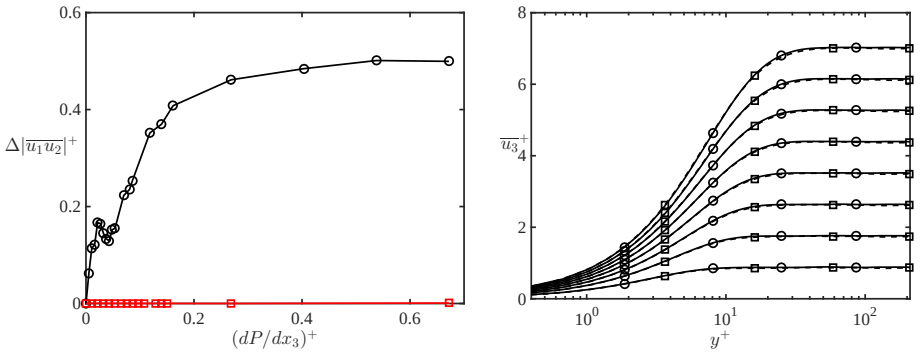

FIGURE 2. Left: circle symbols, sensitivity of $\Delta|\overline{u_1u_2}|^+ \equiv \max\left[|\overline{u_1u_2}|^+(t) - |\overline{u_1u_2}|^+(0)\right]$ to $(\mathrm{d}P/\mathrm{d}x_3)^+$. Squared symbols, sensitivity of $\Delta|\overline{u_1u_2}|^+$ to $(\mathrm{d}P/\mathrm{d}x_3)^+$ with zero Neumann boundary condition for the instantaneous u_3 velocity component. Each case corresponds to a channel flow simulation with initial $Re_\tau = 186$. A total time-transient of one eddy turnover time based on the streamwise friction velocity is considered $T^* = 1$. Right: time-evolution of the spanwise velocity profile for the $Re_\tau = 186$ (circle symbols) and $Re_\tau = 546$ (squared symbols) cases, both characterized by $(\mathrm{d}P/\mathrm{d}x_3)^* = w_\tau^{2+} = 40$.

2.2.2. *Viscous and inviscid effects of a sudden mean spanwise pressure gradient*

In this section we want to gain further insight into the problem by determining the dependence of the maximum drop in $|\overline{u_1u_2}|$ on the imposed $\mathrm{d}P/\mathrm{d}x_3$, and to determine whether this is caused by the acceleration term $d\overline{u_3}/dt$, or induced by emergence of a strong shear layer due to near-wall viscous effects. The analysis will consider a time-transient of total duration $T^+ = 186$, corresponding to one eddy turnover time for the lower Re_τ cases. This will shed further light on the problem at hand and inform a future analysis of the flow system based on rapid distortion theory (Hunt & Carruthers 1990).

Figure 2 features the sensitivity of the maximum drop in $|\overline{u_1u_2}|^+$ to $(\mathrm{d}P/\mathrm{d}x_3)^+$ during the initial transient of duration $T^+ = 186$. With the exception of a local maximum at $(\mathrm{d}P/\mathrm{d}x_3)^+ \approx 0.02$, $\Delta|\overline{u_1u_2}|^+$ tends to increase monotonically with $(\mathrm{d}P/\mathrm{d}x_3)^+$ in the considered range, with stronger gradients for $(\mathrm{d}P/\mathrm{d}x_3)^+ \lesssim 0.2$. Current results indicate that the maximum drop in $|\overline{u_1u_2}|^+$ is likely to asymptote to a constant of $\Delta|\overline{u_1u_2}|^+ \approx 0.5$ for $(\mathrm{d}P/\mathrm{d}x_3)^+ \gtrapprox 0.6$. Note that the runs characterized by a large $(\mathrm{d}P/\mathrm{d}x_3)^+$ do not entirely satisfy the DNS resolvability condition at the end of the time-transient, and further analysis is required to fully confirm the observed asymptotic trend.

To isolate viscous effects from those induced by the spanwise acceleration $d\overline{u_3}/dt$, a series of runs are performed were a free-slip boundary condition is enforced for the u_3 velocity component rather than the canonical no-slip. This "trick" will result in an accelerated plug flow in the spanwise direction, where wall-blocking effects are present, but no spanwise shear layer will grow from the wall. Results from such tests are featured in Figure 2. As is apparent, spanwise acceleration alone does not yield an appreciable drop in $|\overline{u_1u_2}|$, highlighting how viscous effects and the related growth of a spanwise shear layer are responsible for the observed behavior.

These findings further support the current theory on transversely strained boundary-layer flows, based on which when an equilibrium (or developing) boundary layer is subjected to rapid spanwise strain, pressure redistribution terms in the u_iu_i budget equations remove energy from the u_1 and u_2 fluctuations and transfer it to the u_3 component (Moin *et al.* 1990; Coleman *et al.* 1996). A reduction in perturbations associated with the lift-up mechanism then yields the observed decrease in the $\overline{u_1u_2}$ Reynolds stress magnitude. A

similar behavior was recently observed in transitional boundary-layer flows subjected to spanwise wall oscillations (Hack & Zaki 2015).

The growth of the spanwise boundary layer δ_3 is initially governed by viscous diffusion, i.e. $\mathrm{d}\delta_3/\mathrm{d}t \sim \sqrt{\nu/t}$, after which turbulent diffusion prevail and $\mathrm{d}\delta_3/\mathrm{d}t \sim w_\tau$. Viscous diffusion scales in inner units, hence runs characterized by different Re_τ but the same w_τ^+ will be characterized by a similar δ_3^+ time-evolution throughout the transient, as confirmed by results featured in Figure 2(b). As stated above, the drop in $|\overline{u_1u_2}|$ occurs in concomitance with the spanwise shear layer. The $|\overline{u_1u_2}|$ deficit is thus expected to originate from the wall and to extend toward the outer layer at a rate dictated by $\mathrm{d}\delta_3/\mathrm{d}t$, as apparent from Figure 1. Note also the excellent collapse of outer-scaled solutions (see Figure 1(b)), which highlights how the initial viscous diffusion phase can be safely neglected throughout the considered cases.

3. Wall modeling of three-dimensional transient channel

In this section, the predictive capabilities of three wall models are examined for the 3D channel flow case at $Re_\tau = 934$.

3.1. *Wall models*

Three wall-stress models are tested in the present work: the non-equilibrium wall models of Park & Moin (2014) and Yang *et al.* (2015), and an equilibrium stress balance model by Kawai & Larsson (2012). Given the LES solution at a fixed distance away from the wall, all these models produce an approximate wall boundary condition for the near-wall underresolved LES in terms of the wall-shear stress. The usual no-slip condition at the wall ceases to produce an accurate estimate of the momentum drain at the wall due to the coarse near-wall grid in LES. Therefore, LES equations are integrated in time using the wall-shear stress provided by the wall model as a Neumann boundary condition.

The non-equilibrium wall model of Park & Moin (2014, 2016) solves the full Navier-Stokes equations on a separate near-wall mesh (wall-model domain) with a mixing-length type eddy-viscosity closure which dynamically accounts for the resolved portion of the turbulence in the wall-model domain. This formulation is the most comprehensive amongst the considered wall-stress models, and accounts for many physical effects embedded in the original Navier-Stokes equations. Herein, this model is termed NEQWM.

The model by Yang *et al.* (2015) accounts for non-equilibrium effects while retaining a moderate modeling complexity. This model assumes a parametric velocity profile in the near-wall region, where the parameters are determined by enforcing a number of physical constraints. These include the continuity of the profile, the LES matching condition at a specified wall distance, and compliance with the vertically integrated momentum equation. This model was named as integral wall model (IWM), as the momentum integral constraint is crucial in accounting for some of the non-equilibrium effects.

Lastly, the equilibrium stress balance model (EQWM) of Kawai & Larsson (2012) is derived from the NEQWM by retaining only the wall-normal diffusion terms. The model consists of a simple ordinary differential equation, which is solved along the wall-normal direction on each wall face (or wall collocation points) (Wang & Moin 2002).

In all the considered wall-layer models, the spanwise pressure forcing term has been accounted for in the formulation, to comply with the outer LES equations. Note that including the spanwise pressure gradient is particularly important for the NEQWM, in order to provide the required dominant balance in the spanwise momentum conservation equation at small t.

The NEQWM and IWM in their original form require proper time averagings performed on the fly. In the NEQWM, in order to avoid the skin-friction overprediction, the resolved turbulent stress is evaluated on the fly, and it is then subtracted from the modeled stress. In the IWM, the wall-model input is averaged in time to regularize the wall-shear stress, which otherwise was found to cause numerical instability. As a statistically unsteady flow is considered in the present work, the time averaging mentioned above is replaced with a spatial average along wall-parallel planes.

3.2. *Numerical setup*

The codes used for wall-modeled calculations are different from the one used for the DNS analysis, mainly because the wall models were available conveniently in other well-validated LES codes. The calculations using the NEQWM and EQWM are conducted using the code CharLES, which is an unstructured-grid finite-volume LES code for compressible flows. The code is second-order accurate in space, but the reconstruction scheme upgrades to a fourth-order accuracy on uniform Cartesian grids. The dynamic Smagorinsky model (Moin *et al.* 1991; Lilly 1992) is used for the closures of the subgrid-scale (SGS) terms in the filtered conservation equations. The bulk Mach number is fixed at 0.2 for comparison to the incompressible reference DNS.

An incompressible half-channel code LESGO is used for the IWM. This code solves the filtered Navier-Stokes equations in a half channel with a staggered grid, using a pseudo-spectral approach in the wall-parallel directions and a second-order central finite difference scheme in the wall-normal direction. A scale-dependent Lagrangian-dynamic Smagorinsky model is used for the SGS closure (Bou-Zeid *et al.* 2005).

Wall-modeled calculations are initialized with a converged two-dimensional channel flow at $Re_\tau = 934$. The LES grid is substantially coarser than the DNS grid. For a domain size $(L_1, L_2, L_3) = (8\pi h, 2h, 3\pi h)$ as in the DNS, a total of 265,980 cells are deployed in LES with $(N_1, N_2, N_3) = (130, 31, 66)$, corresponding to a grid solution in wall units of $(\Delta_1^+, \Delta_2^+, \Delta_3^+) = (180,\ 60,\ 133)$ based on the friction velocity of the initial 2D channel flow. A spanwise pressure gradient, which is ten times larger than the streamwise pressure gradient, is applied to induce a cross-stream shear layer which grows in time from the wall toward the channel centerline. Simulations are run for one eddy-turnover time based on the streamwise friction velocity ($tu_\tau/h \approx 1$). The friction Reynolds number at the final time is slightly smaller than 1100. The location where the LES data are fed to the wall models is fixed at the centroids of the third cell away from the walls ($x_2/h \approx 0.16$). The wall models grids, if any, have the same wall-parallel content as that of the LES grid, with 30$\sim$40 cells stretched along the wall-normal direction to resolve the sublayer.

3.3. *Results and discussion*

Performance of WMLES is dictated largely by the wall-shear stress content from wall models. Figure 3 features the time-evolution of the streamwise and spanwise mean wall-stress components ($\overline{\tau_1}$ and $\overline{\tau_3}$, respectively), normalized by the reference 2D value. A general observation from Figure 3(a) is that the NEQWM produces a very accurate prediction of the $\overline{\tau_3}$ time-evolution, throughout the considered transient. The EQWM and the IWM are not able to capture the rapid initial increase in the normalized $\overline{\tau_3}$, resulting in up to 50% and 25% underprediction throughout the initial transient ($tu_\tau/h \lesssim 0.2$), respectively, compared to the DNS. The EQWM and the IWM still correctly capture the $\overline{\tau_3}$ growth rate for $tu_\tau/h \gtrsim 0.1$, resulting in errors of 10% and 2%, respectively, at the end of the considered transient ($tu_\tau/h = 1$).

$\overline{\tau_1}$ predicted from the wall models is in relatively good agreement with the corre-

sponding DNS values (Figure 3(b)). The EQWM and the IWM show up to 5% and 2% deviations respectively throughout the transient. The NEQWM predicts a relatively faster variation in $\overline{\tau_1}$ for $tu_\tau/h \lesssim 0.4$ when compared the other wall-layer models, but deviation from the DNS result is modest (up to 7%) and it rapidly reduces as time advances. The theoretical underpinning for such a rapid response in $\overline{\tau_1}$ when the NEQWM is used requires further analysis and will be the subject of future work.

Time-evolution of the wall-shear angle, defined as $\alpha = \tan^{-1}(\overline{\tau_3}/\overline{\tau_1})$, is shown in Figure 4($a$). Performance of wall models here is similar as in $\overline{\tau_3}$. Such a behavior is explained when noting that relative time-variations in $\overline{\tau_1}$ are modest when compared to corresponding variations in $\overline{\tau_3}$. Accurate prediction of the wall-shear angle (or flow direction near the wall) is of some importance in external flows over wings or bluff bodies, as it can directly affect the force exerted on the bodies through modification of circulation, downwash effect, pressure distribution, and strength of separation. We anticipate that the NEQWM, which predicts $\overline{\tau_3}$ and α much more accurately, would outperform the EQWM and the IWM in such situations.

As expected, none of the wall-modeled LES is able to reproduce the initial reduction in $|\overline{\tau_1}|$, occurring at $tu_\tau/h \lesssim 0.4$. Such a decrease in the streamwise wall-stress component results from the complex flow dynamics that characterize 3DTBLs, as described in Section 2. The considered wall-layer models are based on the eddy viscosity assumption, which predicts increasing shear rates as additional strain rates are applied to the flow. It hence comes at no surprise that the WMLES cases consistently feature an approximately monotonic increase in $|\overline{\tau_1}|$ after a sudden spanwise pressure gradient is applied, resulting from the additional transverse straining of the flow in the near-wall region. Despite such a limitation, results are in agreement with the expectation that wall models with a higher degree of modeling complexity would produce more accurate results in complex flows.

Figure 4(b) shows the development of the mean spanwise velocity over one eddy-turnover time. It is observed that turbulence diffuses from the wall to the center line with increasing time, as described in Section 2. The initial spanwise velocity profile starts to develop its own logarithmic region at later times ($tu_\tau/h > 0.6$), although its slope is substantially smaller than that of the standard log-layer in equilibrium channel flows. At distances from the wall that scale with the thickness of the spanwise boundary-layer (δ_3), $\overline{u_3}$ is essentially an accelerated plug flow, characterized by $\mathrm{d}\overline{u_3}/\mathrm{d}t \approx (\mathrm{d}P/\mathrm{d}x_3)t$. As expected, all the considered WMLESs provide an excellent prediction of such a trivial flow. Very good agreement between DNS and WMLESs is also observed in the turbulent flow region, where a spanwise logarithmic layer forms, and where contributions from the LES closure and the wall-layer models are expected to play a role in the mean spanwise momentum balance. This findings highlight how the considered WMLES are capable of accurately predicting the mean spanwise velocity profile that arises in response to the proposed transverse pressure perturbation ($\mathrm{d}P/\mathrm{d}x_3 = 10\mathrm{d}P/\mathrm{d}x_1$). Although not shown here because of space limitations, the mean streamwise velocity changed little in time from its initial 2D state, and good agreement with the DNS was found throughout the wall-modeled calculations.

Overall, the more comprehensive, PDE-based, NEQWM outperforms the EQWM and IWM for the considered flow system. This observation is in agreement with findings from Wang & Moin (2002) and Park (2017), who showed that the accuracy of WMLES in complex flows can be improved by accounting for more of the non-equilibrium effects.

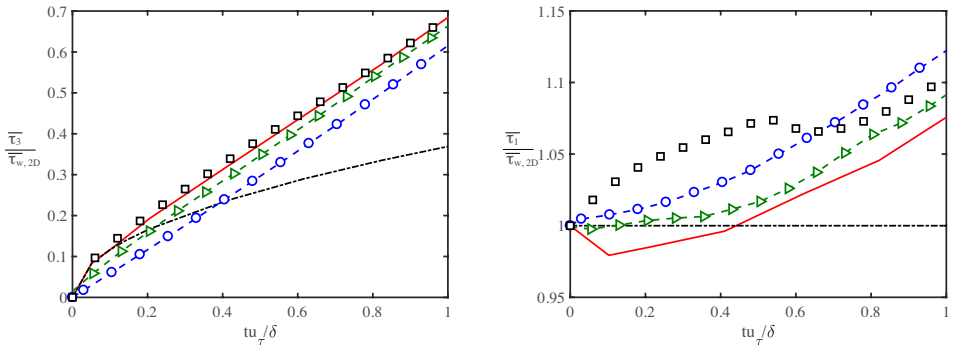

FIGURE 3. Time history of the mean spanwise ($\overline{\tau_3}$, left) and streamwise ($\overline{\tau_1}$, right) wall shear-stress vector components from WMLESs and the DNS. Both terms have been normalized by the initial 2D wall shear-stress value ($\overline{\tau_{w,2D}}$). Red solid line, DNS; square symbols, WMLES (NEQWM); triangle symbols, WMLES (IWM); circle symbols, WMLES (EWQM); black dash-dotted line, laminar solution.

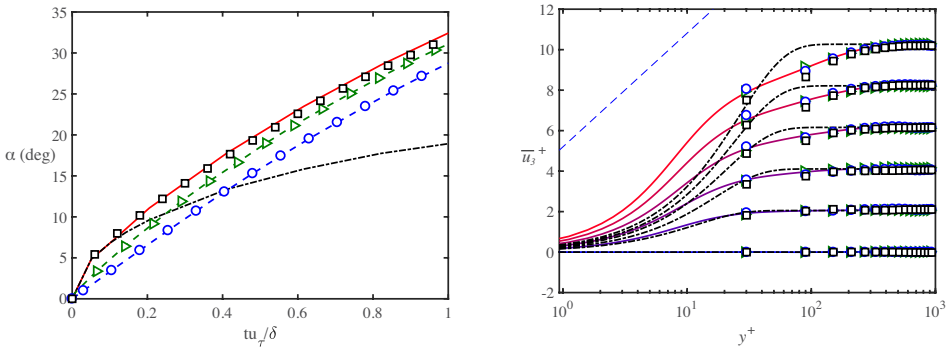

FIGURE 4. Left: Wall shear-stress angle, $\alpha \equiv \tan^{-1}(\overline{\tau_3}/\overline{\tau_1})$. See Figure 3 for a reference to colors and symbols. Right: Mean spanwise velocity at $t^* = 0$, 0.21, 0.405, 0.615, 0.825, and 1.02 (from bottom to top). Red solid line, DNS; square symbols, WMLES (NEWQM); triangle symbols, WMLES (IWM); circle symbols, WMLES (EWQM); black dash-dotted line, laminar solution; blue dashed line, standard log law ($\overline{u_3}^+ = (1/0.41)\ln x_2^+ + 5.2$). Normalization of the variables are done with the kinematic viscosity and the friction velocity of the initial 2D flow.

4. Conclusions

A series of DNS of fully-developed incompressible planar channel flow have been performed, with focus on the initial transient after a sudden transverse pressure gradient is applied. Three Reynolds numbers have been considered, namely $Re_\tau = 186$, $Re_\tau = 546$ and $Re_\tau = 934$, to gain insight for the first time on inner and outer scaling of the problem. It is shown that the considered statistics ($\overline{u_3}, \overline{u_1 u_2}$) collapse in the near-wall region [$x_2^+ = \mathcal{O}(1)$] across simulations characterized by different Re_τ but the same $(\mathrm{d}P/\mathrm{d}x_3)^+ \equiv w_\tau^{2+}/Re_\tau$ when scaled in inner units. Conversely, statistics collapse in the outer layer $x_2/h = \mathcal{O}(1)$ for runs at different Re_τ but the same w_τ/u_τ when scaled in outer units. The proposed scaling provides the ideal framework for future comparison of Reynolds numbers effects on 3D channel flow simulations.

A series of spanwise pressure gradients have been considered for the lower Re_τ value, to test the sensitivity of the observed $|\overline{u_1u_2}|$ deficit to the spanwise forcing parameter during a transient of total duration $tu_\tau/h = 1$. the $|\overline{u_1u_2}|$ deficit is characterized by a local maximum at $(\mathrm{d}P/\mathrm{d}x_3)^+ \approx 0.02$, and asymptotes to a constant for $(\mathrm{d}P/\mathrm{d}x_3)^+ \gtrsim 0.6$. An additional series of DNSs have been performed with a free-slip wall boundary condition applied to the $\overline{u_3}$ velocity component, resulting in an accelerated plug flow in the spanwise direction. Under such settings, no apparent deficit in $|\overline{u_1u_2}|$ is observed during the transient, hence the spanwise shear layer developing from the wall is to be regarded as the responsible for the observed counter-intuitive behavior. Such findings provide evidence in support of the current theory on transversely strained boundary layers, based on which intercomponent transfer of turbulent energy via pressure-strain is responsible to diminish $|\overline{u_2u_2}|$ in response to rapid spanwise straining. This yields a reduction in mean shear production of $\overline{u_1u_2}$, thus supporting the observed deficit in $|\overline{u_1u_2}|$.

Further, the predictive capabilities of three state-of-the-art wall-modeling techniques for LES have been assessed for the considered flow system, with focus on the highest among the Re_τ cases. Wall models with a higher degree of modeling complexity yield a more accurate prediction of the mean wall-shear. For instance, LES with the NEQWM predicts very accurately the magnitude of the spanwise mean wall-shear component, as well as the angle of the mean wall-shear vector. Conversely, the EQWM and IWM are not able to capture the rapid initial increase in the spanwise wall-shear magnitude, resulting in deviations up to 50% and 25 % respectively at small times. At larger times, however, both models are in relatively good agreement with DNS results and with predictions from the NEQWM. As expected, none of the considered wall-layer models is able to account for the observed initial $|\overline{u_1u_2}|$ deficit, due to the very nature of eddy-viscosity formulations. These findings highlight how the accuracy of WMLES in three dimensional transient boundary layers can be improved by accounting for non-equilibrium effects, and set the ground for a better understanding and future developments in terms of wall-layer models for complex flows.

Acknowledgments

This investigation was funded by ONR, Grant #N00014-16-S-BA10.

REFERENCES

Bose, S. & Park, G. I. 2018 Wall-modeled LES for complex turbulent flows. *Annu. Rev. Fluid Mech.* **50** (In Press).

Bou-Zeid, E., Meneveau, C. & Parlange, M. B. 2005 A scale-dependent Lagrangian dynamic model for large eddy simulation of complex turbulent flows. *Phys. Fluids* **17**, 025105.

Chapman, D. 1979 Computational aerodynamics development and outlook. *AIAA J.* **12**, 1293–1313.

Choi, H. & Moin, P. 2012 Grid-point requirements for large eddy simulation: Chapman's estimates revisited. *Phys. Fluids* **24**, 011702.

Chorin, A. J. 1968 Numerical solution of the Navier-Stokes equations. *Math. Comput.* **22**, 745–762.

Coleman, G. N., Kim, J. & Le, A.-T. 1996 A numerical study of three-dimensional wall-bounded flows. *Int. J. Heat Fluid Flow* **17**, 333–342.

Coleman, G. N. & Spalart, P. R. 1996 Direct numerical simulation of strained three-dimensional wall-bounded flows. *Environ. Therm. Fluid. Sci.* **13**, 239–251.

Cossu, C. & Hwang, Y. 2017 Self-sustaining processes at all scales in wall-bounded turbulent shear flows. *Phil. Trans. R. Soc. A* **375** 2088.

Flores, O. & Jiménez, J. 2010 Hierarchy of minimal flow units in the logarithmic layer. *Phys. Fluids* **22**, 071704.

Hack, M. J. P. & Zaki, T. A. 2015 Modal and non-modal stability of boundary layers forced by spanwise wall oscillations. *J. Fluid Mech.* **778**, 389–427.

Hunt, J. C. R. & Carruthers, D. J. 1990 Rapid distortion theory and the "problems" of turbulence. *J. Fluid Mech.* **212**, 497–532.

Hwang, Y. & Cossu, C. 2011 Self-sustained processes in the logarithmic layer of turbulent channel flows. *Phys. Fluids* **23** 061702.

Jiménez, J. & Pinelli, A. 1999 The autonomous cycle of near-wall turbulence. *J. Fluid Mech.* **389**, 335–359.

Johnston, J. P. & Flack, K. A. 1996 Review ? Advances in three-dimensional turbulent boundary layers with emphasis on the wall-layer regions. *J. Fluids Eng.* **118**, 219–232.

Kawai, S. & Larsson, J. 2012 Wall-modeling in large eddy simulation: length scales, grid resolution, and accuracy. *Phys. Fluids* **24**, 015015.

Kiesow, R. O. & Plesniak, M. W. 2003 Near-wall physics of a shear-driven three-dimensional turbulent boundary layer with varying crossflow. *J. Fluid Mech.* **484**, 1–39.

Klewicki, J., Fife, P., Wei, T. & McMurtry, P. 2007 A physical model of the turbulent boundary layer consonant with mean momentum balance structure. *Philos. Trans. A Math. Phys. Eng. Sci.* **365**, 823–839.

Larsson, J., Kawai, S., Bodart, J. & Bermejo-Moreno, I. 2016 Large eddy simulation with modeled wall-stress: recent progress and future directions. *Mech. Eng. Rev.* **3**, 1–23.

Lilly, D. K. 1992 A proposed modification of the Germano subgrid-scale closure method. *Phys. Fluids* **4**, 633–635.

Littell, H. S. & Eaton, J. K. 1994 Turbulence characteristics of the boundary layer on a rotating disk. *J. Fluid Mech.* **266**, 175–207.

Lozano-Durán, A., Flores, O. & Jiménez, J. 2012 The three-dimensional structure of momentum transfer in turbulent channels. *J. Fluid Mech.* **694**, 100–130.

Lozano-Durán, A. & Jiménez, J. 2014 Time-resolved evolution of coherent structures in turbulent channels: characterization of eddies and cascades. *J. Fluid Mech.* **759**, 432–471.

Maciel, Y., Rossignol, K.-S. & Lemay, J. 2006 Self-similarity in the outer region of adverse-pressure-gradient turbulent boundary layers. *AIAA J.* **44**, 2450–2464.

Moin, P., Shih, T. H., Driver, D. & Mansour, N. N. 1990 Direct numerical simulation of a three-dimensional turbulent boundary layer. *Phys. Fluids* **2**, 1846–1853.

Moin, P., Squires, K., Cabot, W. & Lee, S. 1991 A dynamic subgrid-scale model for compressible turbulence and scalar transport. *Phys. Fluids* **3**, 2746–2757.

Orlandi, P. 2000 *Fluid flow phenomena: A numerical toolkit.* Springer Science & Business Media.

Panton, R. L. 2001 Overview of the self-sustaining mechanisms of wall turbulence. *Prog. Aerosp. Sci.* **37**, 341–383.

Park, G. I. 2017 Wall-modeled large-eddy simulation of a high Reynolds number separating and reattaching flow. *AIAA J.* **55**, pp. 3709 – 3721.

Park, G. I. & Moin, P. 2014 An improved dynamic non-equilibrium wall-model for large eddy simulation. *Phys. Fluids* **26**, 015108.

Park, G. I. & Moin, P. 2016 Numerical aspects and implementation of a two-layer zonal wall model for LES of compressible turbulent flows on unstructured meshes. *J. Comput. Phys.* **305**, 589–603.

Piomelli, U. & Balaras, E. 2002 Wall-layer models for large-eddy simulations. *Annu. Rev. Fluid Mech.* **34**, 349–374.

Spalart, P. R. 1989 Theoretical and numerical study of a three-dimensional turbulent boundary layer. *J. Fluid Mech.* **205**, 319–340.

Townsend, A. A. 1961 Equilibrium layers and wall turbulence. *J. Fluid Mech.* **11**, 97–120.

Wang, M. & Moin, P. 2002 Dynamic wall modeling for large-eddy simulation of complex turbulent flows. *Phys. Fluids* **14**, 2043–2051.

Wray, A. A. 1990 *Minimal-storage time advancement schemes for spectral methods.* Unpublished report, NASA Ames Research Center.

Wu, X. & Squires, K. D. 2000 Prediction and investigation of the turbulent flow over a rotating disk. *J. Fluid Mech.* **418**, 231–264.

Yang, X. I. A., Sadique, J., Mittal, R. & Meneveau, C. 2015 Integral wall model for large eddy simulations of wall-bounded turbulent flows. *Phys. Fluids* **27**, 025112.